Noncanonical imprinting sustains embryonic development and restrains placental overgrowth

Shogo Matoba,[1,2,10] Chisayo Kozuka,[3,10] Kento Miura,[1,4] Kimiko Inoue,[1,5] Mami Kumon,[3] Ryoya Hayashi,[3,6] Tatsuya Ohhata,[7] Atsuo Ogura,[1,5,8,9] and Azusa Inoue[3,6,10]

[1]Bioresource Engineering Division, RIKEN Bioresource Research Center, Tsukuba 305-0074, Japan; [2]Cooperative Division of Veterinary Sciences, Tokyo University of Agriculture and Technology, Fuchu 183-8509, Japan; [3]Young Chief Investigator (YCI) Laboratory for Metabolic Epigenetics, RIKEN Center for Integrative Medical Sciences, Yokohama 230-0045, Japan; [4]Department of Disease Model, Research Institute of Radiation Biology and Medicine, Hiroshima University, Hiroshima 734-8553, Japan; [5]Graduate School of Life and Environmental Sciences, University of Tsukuba, Tsukuba 305-8572, Japan; [6]Tokyo Metropolitan University, Hachioji 192-0397, Japan; [7]Department of Molecular Biology, Hamamatsu University School of Medicine, Hamamatsu 431-3192, Japan; [8]The Center for Disease Biology and Integrative Medicine, Faculty of Medicine, University of Tokyo, Tokyo 113-0033, Japan; [9]RIKEN Cluster for Pioneering Research, Wako 351-0198, Japan

Genomic imprinting regulates parental origin-dependent monoallelic gene expression. It is mediated by either germline differential methylation of DNA (canonical imprinting) or oocyte-derived H3K27me3 (noncanonical imprinting) in mice. Depletion of Eed, an essential component of Polycomb repressive complex 2, results in genome-wide loss of H3K27me3 in oocytes, which causes loss of noncanonical imprinting (LOI) in embryos. Although *Eed* maternal KO (matKO) embryos show partial lethality after implantation, it is unknown whether LOI itself contributes to the developmental phenotypes of these embryos, which makes it unclear whether noncanonical imprinting is developmentally relevant. Here, by combinatorial matKO of *Xist*, a noncanonical imprinted gene whose LOI causes aberrant transient maternal X-chromosome inactivation (XCI) at preimplantation, we show that prevention of the transient maternal XCI greatly restores the development of *Eed* matKO embryos. Moreover, we found that the placentae of *Eed* matKO embryos are remarkably enlarged in a manner independent of *Xist* LOI. Heterozygous deletion screening of individual autosomal noncanonical imprinted genes suggests that LOI of the *Sfmbt2* miRNA cluster chromosome 2 miRNA cluster (C2MC), solute carrier family 38 member 4 (*Slc38a4*), and *Gm32885* contributes to the placental enlargement. Taken together, our study provides evidence that *Xist* imprinting sustains embryonic development and that autosomal noncanonical imprinting restrains placental overgrowth.

[*Keywords*: genomic imprinting; *Xist*; X-chromosome inactivation; mouse embryo; placenta]

Supplemental material is available for this article.

Received January 16, 2022; revised version accepted April 8, 2022.

Genomic imprinting is regulated by germline DNA methylation-dependent and -independent mechanisms, which are respectively termed canonical and noncanonical imprinting (Tucci et al. 2019; Chen and Zhang 2020). In noncanonical imprinting, maternal H3K27me3 is deposited over broad domains during oogenesis, is inherited by early embryos, and represses maternal gene expression of dozens of paternally expressed genes (PEGs) in mouse preimplantation embryos (Inoue et al. 2017a,b; Santini et al. 2021). Maternal H3K27me3 domains are largely lost after implantation, but some of the PEGs maintain their allele-specific expression in the extraembryonic cell lineage by acquiring secondary DNA methylation at the repressive maternal allele in a G9a- and Dnmt3a/3b-dependent fashion (Chen et al. 2019; Hanna et al. 2019; Andergassen et al. 2021; Zeng et al. 2021). So far, at least seven autosomal PEGs (growth factor receptor bound protein 2-associated protein 1 [*Gab1*], *Gm32885*, jade family PHD finger 1 [*Jade1/Phf17*], pluripotency associated transcript 20 [*Platr20*], Scm-like with four mbt domains 2 [*Sfmbt2*], *Slc38a4*, and SPARC-related modular calcium binding 1 [*Smoc1*]) and an X-linked gene, *Xist*, have been identified as noncanonical imprinted genes that maintain paternal

[10]These authors contributed equally to this work.
Corresponding author: azusa.inoue@riken.jp
Article published online ahead of print. Article and publication date are online at http://www.genesdev.org/cgi/doi/10.1101/gad.349390.122.

expression after implantation (Chen and Zhang 2020; Hanna and Kelsey 2021; Kobayashi 2021; Raas et al. 2022).

The functions of noncanonical imprinting remain elusive. In previous studies, noncanonical imprinting was disrupted by oocyte-specific knockout of *Eed*, an essential component of Polycomb repressive complex 2 (PRC2) (Inoue et al. 2018; Chen et al. 2019; Harris et al. 2019). *Eed* KO oocytes show genome-wide loss of H3K27me3. Following fertilization with wild-type sperm, *Eed* maternal KO (matKO) embryos exhibit biallelic expression of noncanonical imprinted genes (Inoue et al. 2018; Chen et al. 2019; Harris et al. 2019). Global loss of H3K27me3 in *Eed* matKO embryos persists until the morula stage, when *Eed* starts to be expressed from the intact paternal allele (Inoue et al. 2018; Harris et al. 2019). Although *Eed* matKO embryos are grossly normal during preimplantation development, they are developmentally retarded by E6.5 and subsequently show prenatal, male-biased, sublethality due to yet to be determined reasons (Inoue et al. 2018; Prokopuk et al. 2018; Harris et al. 2019). This lethality is not due to *Eed* haploinsufficiency, because *Eed* heterozygous ($Eed^{+/\Delta}$) embryos derived from $Eed^{+/\Delta}$ dams normally develop to term (Prokopuk et al. 2018). These studies suggest that developmental defects of *Eed* matKO embryos may be caused by loss of noncanonical imprinting (LOI). However, it is equally possible that these defects are caused by the other effects accompanied by genome-wide loss of H3K27me3 during oogenesis and early preimplantation development. For example, a recent study reported that Polycomb-associating higher-order chromatin structure is attenuated in *Eed* matKO embryos (Du et al. 2020), raising the possibility that LOI may be irrelevant to the developmental abnormalities in these embryos. To understand the functions of noncanonical imprinting, it is necessary to separate the effects of LOI and global H3K27me3 loss in *Eed* matKO embryos.

Xist is a candidate noncanonical imprinted gene whose LOI might cause embryonic lethality. *Xist* encodes a long noncoding RNA that spreads across the X chromosome in *cis* and induces X-chromosome inactivation (XCI) (Augui et al. 2011; Lee and Bartolomei 2013; Loda et al. 2022). In mouse preimplantation embryos and the extraembryonic tissues, the paternal X chromosome (Xp) is selectively inactivated. For this to occur, *Xist* on the maternal X chromosome (Xm) is silenced by H3K27me3 during preimplantation development (Fig. 1; Inoue et al. 2017b). Loss of maternal H3K27me3 in the *Eed* matKO results in ectopic expression of *Xist* from Xm, leading to down-regulation of Xm-linked genes in morula embryos (Inoue et al. 2018; Harris et al. 2019). Nevertheless, the *Xist* derepression and the aberrant Xm inactivation are resolved by the late blastocyst stage (Fig. 1; Inoue et al. 2018; Harris et al. 2019). Thus, *Xist* LOI-mediated aberrant XCI in *Eed* matKO embryos is transient at preimplantation. This fact makes it unclear whether *Xist* LOI causes postimplantation lethality.

To address whether *Xist* LOI is responsible for the lethality of *Eed* matKO embryos, we attempted to prevent ectopic expression of *Xist* in *Eed* matKO embryos. To this end, we generated oocyte-specific conditional double KO (DKO) of *Eed* and *Xist*. Maternal expression of *Xist* was expected to be prevented in the *Eed*/*Xist* maternal DKO (matDKO) embryos (Fig. 1). Studies of these embryos allowed us to discriminate between *Xist*-dependent and -independent functions of noncanonical imprinting, which led us to discover the importance of imprints at *Xist* and several autosomal noncanonical imprinted genes for embryonic and placental development, respectively.

Results

To prevent ectopic *Xist* expression from Xm in *Eed* matKO embryos, we generated oocyte-specific DKO of *Eed* and *Xist* by breeding a *Gdf9-Cre*/*Eed* flox (fl) mouse line (Inoue et al. 2018) with an *Xist* flox mouse line (Csankovszki et al. 1999). The *Gdf9-Cre* is an oocyte-specific Cre line in which Cre is expressed from a very early stage of oocyte growth (Lan et al. 2004). Consequently, we obtained $Eed^{fl/fl}/Xist^{fl/fl}$ (termed WT [wild type]), *Gdf9-Cre*/$Eed^{fl/fl}/Xist^{WT/WT}$ (termed *Eed* KO), and *Gdf9-Cre*/$Eed^{fl/fl}/Xist^{fl/fl}$ (termed *Eed*/*Xist* DKO) females (Fig. 1). Immunostaining (IF) analysis confirmed the loss of H3K27me3 and EED in both *Eed* KO and *Eed*/*Xist* DKO fully grown oocytes (FGOs) (Supplemental Fig. S1A,B).

By fertilization with WT sperm, we made WT, *Eed* matKO, and *Eed*/*Xist* matDKO embryos from WT, *Eed* KO, and *Eed*/*Xist* DKO oocytes, respectively. To validate

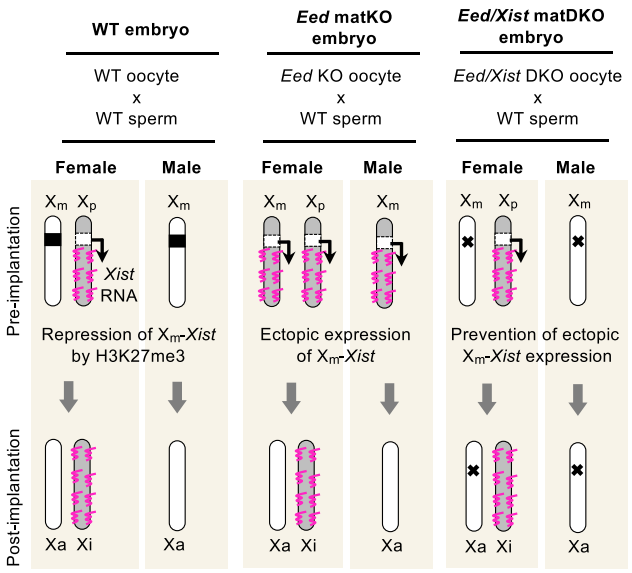

Figure 1. Schematic illustration of the dynamics of *Xist* expression and X-chromosome inactivation (XCI). In WT embryos, *Xist* on the maternal X chromosome (Xm) is silenced by oocyte-derived maternal H3K27me3, allowing *Xist* expression only from the paternal X chromosome (Xp), which becomes inactive X (Xi). In *Eed* matKO embryos, *Xist* on Xm is derepressed at preimplantation, resulting in transient Xm inactivation. Nevertheless, this aberrant XCI state is resolved at the late blastocyst stage, which leads to a proper XCI state in postimplantation embryos. In *Eed*/*Xist* matDKO embryos, it is expected that ectopic expression of *Xist* from Xm is prevented.

the prevention of ectopic *Xist* expression in *Eed/Xist* matDKO embryos, we performed *Xist* RNA-FISH analyses at the morula stage. Simultaneous DNA-FISH using a BAC X-chromosome probe allowed discrimination of male and female embryos (Inoue et al. 2017b). This analysis demonstrated that *Xist* is biallelically and monoallelically expressed in *Eed* matKO and *Eed/Xist* matDKO female embryos, respectively (Fig. 2A,B). Similarly, *Xist* was expressed from Xm in *Eed* matKO but not *Eed/Xist* matDKO male embryos (Fig. 2A,B). To further validate that ectopic XCI is prevented in *Eed/Xist* matDKO embryos, we performed allelic RNA-seq analysis in morula embryos generated by using PWK strain sperms. As expected, down-regulation of Xm-linked genes, which was observed in *Eed* matKO, was completely inhibited in *Eed/Xist* matDKO (Fig. 2C,D; Supplemental Table S1). Additionally, we confirmed that loss of paternal expression biases of H3K27me3-dependent PEGs is commonly observed in *Eed* matKO and *Eed/Xist* matDKO embryos (Supplemental Fig. S1C). These results demonstrate that LOI-induced ectopic expression of *Xist* and aberrant maternal XCI are successfully prevented in *Eed/Xist* matDKO embryos.

To determine whether *Xist* LOI is a cause of developmental retardation observed in *Eed* matKO postimplantation embryos, we dissected embryos at E6.5. As reported previously (Inoue et al. 2018), the average size of *Eed* matKO embryos was significantly smaller than that of WT embryos, although the average number of

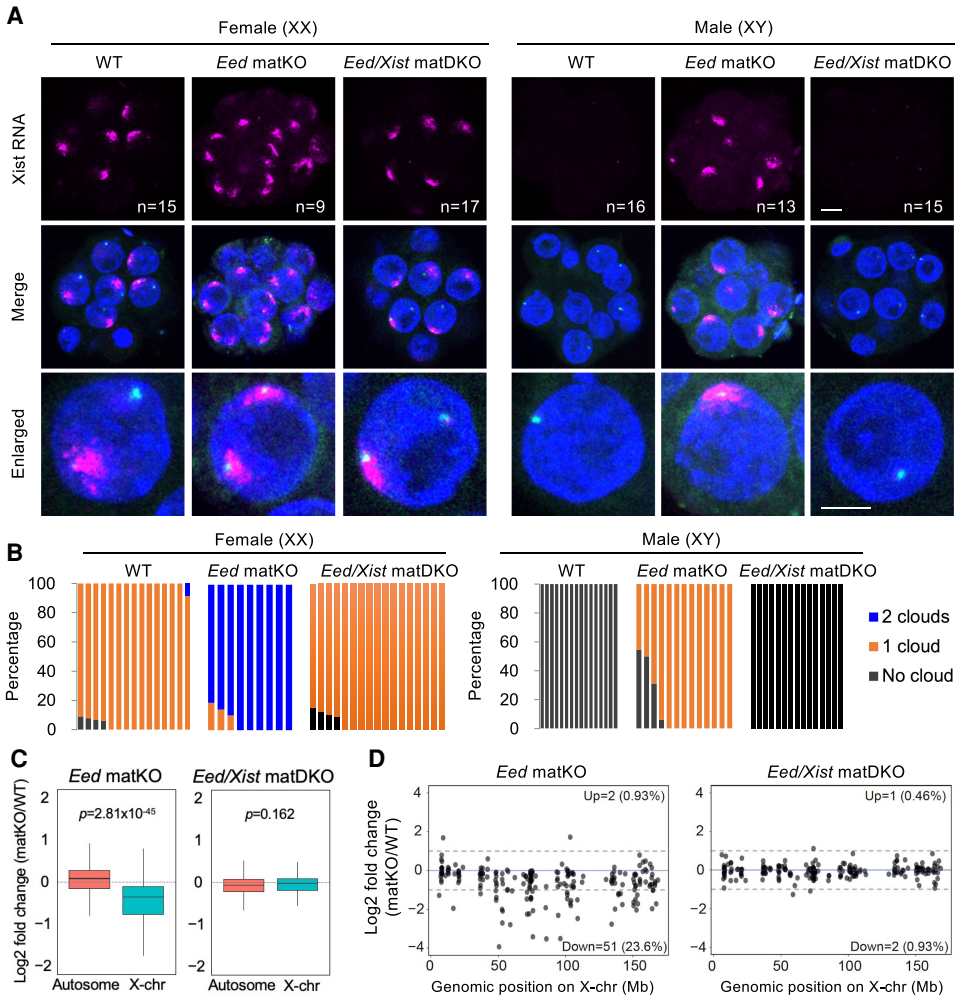

Figure 2. Maternal XCI is prevented in *Eed/Xist* maternal doubleKO (matDKO) embryos. (*A*) Representative images of *Xist* RNA-FISH in morula embryos. The sex of each embryo was assessed by simultaneous DNA-FISH to detect the *Atrx* locus on the X chromosome (green spots). Blue indicates DNA stained with DAPI. The numbers of embryos examined (*n*) are indicated. Scale bars, 10 µm. (*B*) The ratios of blastomeres showing the indicated numbers of *Xist* RNA clouds. Each bar represents an individual embryo. (*C*) Box plot showing the relative expression (matKO/WT) of genes on the maternal autosomes and the maternal X chromosome, respectively, in morula embryos. Genes with ≥20 SNP-containing reads in all replicates were analyzed. The *middle* lines in the boxes represent the medians. Box edges and whiskers indicate the 25th/75th and ±1.5 × interquartile range, respectively. *P*, Mann–Whitney–Wilcoxon test. (*D*) The relative expression (matKO/WT) of individual maternal X-linked genes with ≥20 SNP-containing reads in all replicates. The total number of genes is 216. The numbers of down-regulated and up-regulated genes with a cutoff of fold change 2 are indicated.

A

Embryo	Mother	Father	No. of litters	No. of implantations (Ave ± SD)	No. of embryos (Ave ± SD)
WT	*Eed*$^{fl/fl}$, *Xist*$^{fl/fl}$	B6	6	51 (8.5 ± 2.9)	49 (8.2 ± 2.9)
***Eed* matKO**	*Gdf9*^{Cre}, *Eed*$^{fl/fl}$, *Xist*$^{+/+}$	B6	4	31 (7.8 ± 3.6)	26 (6.5 ± 3.1)
***Eed/Xist* matDKO**	*Gdf9*^{Cre}, *Eed*$^{fl/fl}$, *Xist*$^{fl/fl}$	B6	10	86 (8.6 ± 1.9)	80 (8.0 ± 1.9)
***Xist* matKO**	*Gdf9*^{Cre}, *Eed*$^{+/+}$, *Xist*$^{fl/fl}$	B6	5	52 (10.4 ± 1.8)	49 (9.8 ± 2.2)

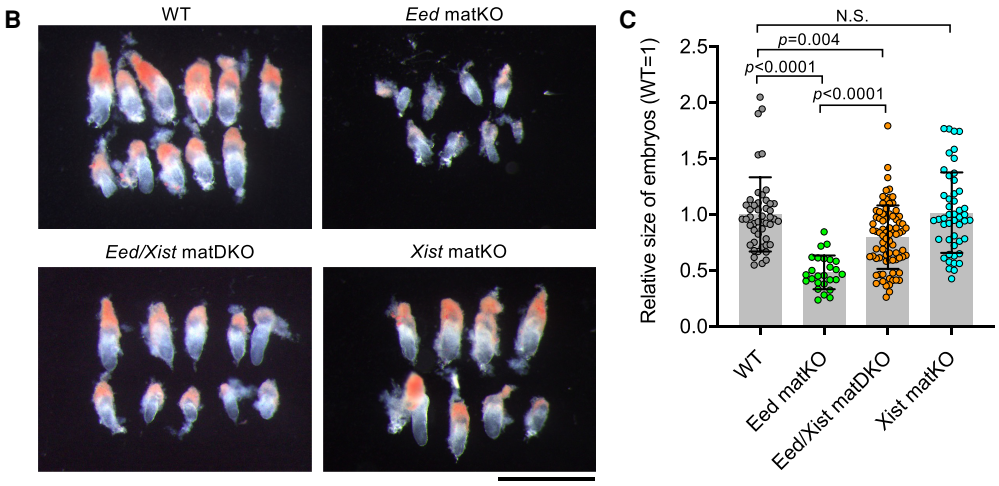

Figure 3. Prevention of maternal XCI at preimplantation largely rescues developmental retardation after implantation. (*A*) Summary table of dissection at E6.5. (*B*) Representative images of E6.5 embryos. Each image represents a single litter. Scale bar, 1 mm. (*C*) Relative sizes of the embryos. The method of quantification is shown in Supplemental Figure S2B. The average size of the WT embryos was set as 1.0. The bars overlaid on the plots indicate mean ± SD. The numbers of embryos examined were 48 WT, 26 *Eed* matKO, 79 *Eed/Xist* matDKO, and 48 *Xist* matKO. *P*, two-tailed Student's *t*-test.

implantations was comparable between *Eed* matKO and WT embryos (Fig. 3A–C; Supplemental Fig. S2A). Importantly, the developmental retardation phenotype was remarkably rescued in *Eed/Xist* matDKO embryos (Fig. 3B, C; Supplemental Fig. S2A,B). This result suggests that *Xist* LOI is largely responsible for the developmental retardation in *Eed* matKO embryos and that transient maternal XCI at preimplantation causes developmental retardation after implantation. Nonetheless, it was also noted that the average size of *Eed/Xist* matDKO embryos was slightly smaller than that of WT embryos (Fig. 3C). This modest retardation was not caused by maternal KO of *Xist*, because the sizes of *Xist* single matKO embryos were comparable with those of WT embryos at E6.5 (Fig. 3B,C; Supplemental Fig. S2A). Therefore, some developmental defects seem to be retained in *Eed/Xist* matDKO embryos.

Next, we conducted caesarian section (C-section) to examine full-term development. As reported previously (Inoue et al. 2018; Prokopuk et al. 2018; Harris et al. 2019), *Eed* matKO embryos showed a high absorption rate (67% per implantation), with the survivors biased to females (Fig. 4A–C). The body weights of *Eed* matKO fetuses were also significantly smaller than those of WT fetuses (Fig. 4D). Importantly, the absorption ratio of *Eed/Xist* matDKO embryos (24% per implantation) was significantly lower than that of *Eed* matKO embryos (Fig. 4A,B). Consistently, the litter size was greatly increased in *Eed/Xist* matDKO, and the body weights of *Eed/Xist* matDKO fetuses were significantly heavier than those of *Eed* matKO fetuses (Fig. 4A,C,D). Additionally, the female bias observed in the surviving *Eed* matKO fetuses was resolved in the *Eed/Xist* matDKO fetuses (Fig. 4A), suggesting that male-biased lethality of *Eed* matKO embryos is caused by *Xist* LOI. These results indicate that *Xist* LOI is the primary cause of embryonic lethality in *Eed* matKO embryos. Nevertheless, the absorption ratio, the litter size, and the body weight of *Eed/Xist* matDKO embryos failed to reach the WT embryo levels (Fig. 4A–D). Again, these modest but nonnegligible defects were not caused by maternal deletion of *Xist*, because they were not observed in *Xist* single matKO embryos (Fig. 4A–D). Additional dissection of *Eed/Xist* matDKO embryos at E10.5 and E13.5 demonstrated that some of the embryos gradually died between E6.5 and E13.5 (Supplemental Fig. S3A,B). The sizes of *Eed/Xist* matDKO embryos were smaller than those of WT embryos at E10.5 and E13.5, while the placental sizes were comparable at E10.5 and slightly larger in *Eed/Xist* matDKO at E13.5 (Supplemental Fig. S3C). Taken together, these results demonstrate that *Xist* LOI is the primary but not the only cause of embryonic lethality of *Eed* matKO embryos.

During these experiments, we found that the placentae of *Eed* matKO concepti were remarkably enlarged at term (Fig. 4E). The placental enlargement phenotype was

A

Embryo	Mother	Father	No. of litters	No. of implantations (Ave ± SD)	No. of absorption (Ave ± SD)	No. of dead fetuses (Ave ± SD)	No. of live fetuses (Ave ± SD)	Sex ratio (Female/ Total)
WT	*Eed*$^{fl/fl}$, *Xist*$^{fl/fl}$	B6	13	128 (9.8 ± 1.9)	16 (1.2 ± 1.7)	1 (0.1 ± 0.3)	111 (8.5 ± 1.7)	0.48
***Eed* matKO**	*Gdf9*^{Cre}, *Eed*$^{fl/fl}$, *Xist*$^{+/+}$	B6	13	117 (9.0 ± 2.2)	79 (5.9 ± 2.5)	6 (0.5 ± 0.1)	32 (2.5 ± 2.0)	0.73
***Eed/Xist* matDKO**	*Gdf9*^{Cre}, *Eed*$^{fl/fl}$, *Xist*$^{fl/fl}$	B6	21	175 (8.2 ± 2.3)	45 (2.0 ± 1.5)	4 (0.2 ± 0.7)	126 (6.0 ± 2.1)	0.53
***Xist* matKO**	*Gdf9*^{Cre}, *Eed*$^{+/+}$, *Xist*$^{fl/fl}$	B6	7	71 (10.1 ± 1.1)	10 (1.4 ± 1.4)	1 (0.1 ± 0.4)	60 (8.6 ± 1.3)	0.47

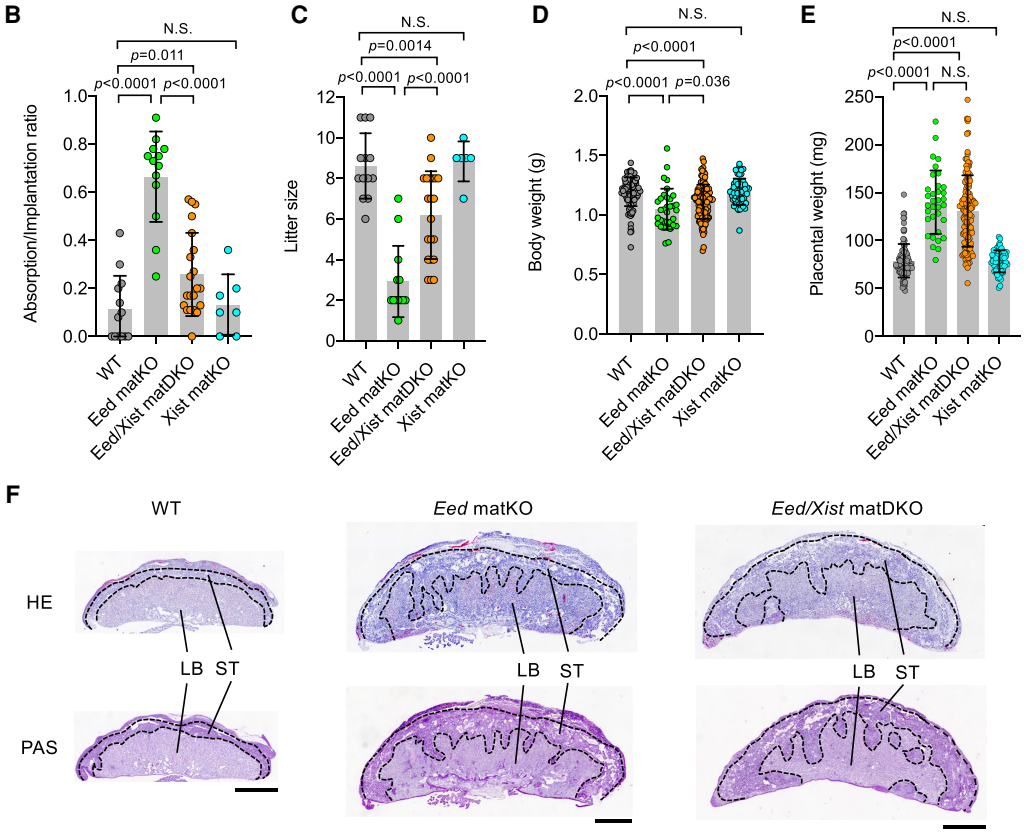

Figure 4. Prevention of transient maternal XCI largely rescues developmental lethality but not placental enlargement. (*A*) Summary table of dissection at E18.5. (*B*) The ratios of the number of absorbed embryos per the number of implantations at E18.5. The bars overlaid on the plots indicate mean ± SD. The number of litters is indicated in *A*. *P*, χ^2 test. (*C–E*) Litter sizes (*C*), body weights (*D*), and placental weights (*E*) at E18.5. The bars overlaid on the plots indicate mean ± SD. The number of litters is indicated in *A*. *P*, two-tailed Student's *t*-test. (*F*) Representative images of placental sections stained with hematoxylin and eosin (HE) and periodic acid Schiff (PAS). (LB) Labyrinthine layer, (ST) spongiotrophoblast layer. Scale bars, 1 mm. The numbers of placentae examined were three WT, three *Eed* matKO, and six *Eed/Xist* matDKO.

not at all restored in *Eed/Xist* matDKO (Fig. 4E), indicating that it is not caused by either *Xist* LOI or the smaller litter size of *Eed* matKO concepti. There was no sex difference in placental weights in *Eed* matKO and *Eed/Xist* matDKO, ruling out a sex-dependent effect (Supplemental Fig. S4A). Histological analysis using hematoxylin and eosin (HE) and periodic acid Schiff (PAS) staining showed that the spongiotrophoblast (ST) layer expanded and invaded into the labyrinth layer in the enlarged placentae (Fig. 4F; Supplemental Fig. S4B), a phenotype indicative of overproliferation of fetal-derived placental cells. These data suggested that noncanonical imprinting might regulate placental growth in an *Xist* imprinting-independent fashion.

Besides *Xist*, there are seven known noncanonical imprinted genes whose imprints are maintained after implantation and lost in *Eed* matKO embryos (Inoue et al. 2018; Chen et al. 2019; Chen and Zhang 2020; Raas et al. 2022). We presumed that biallelic expression of these imprinted genes might be responsible for placental

enlargement in *Eed* matKO and *Eed/Xist* matDKO concepti. To address this possibility, we designed a genetic rescue experiment in which individual noncanonical imprinted genes are fixed to be monoallelically expressed in *Eed/Xist* matDKO embryos. To this end, we prepared heterozygous deletion mutants of the seven autosomal noncanonical imprinted genes: *Gab1*$^{+/\Delta}$, *Gm32885*$^{+/\Delta}$, *Jade1*$^{+/\Delta}$, *Platr20*$^{+/\Delta}$, *Sfmbt2*$^{+/\Delta}$, *Slc38a4*$^{+/\Delta}$, and *Smoc1*$^{+/\Delta}$ (see the Materials and Methods; Supplemental Fig. S5A,B). Since the *Sfmbt2* gene harbors the chromosome 2 miRNA cluster (C2MC) within its intron, which is coimprinted with the host gene (Inoue et al. 2017c; Zeng et al. 2021), C2MC$^{+/\Delta}$ and *Sfmbt2*-coding sequence (CDS)$^{+/\Delta}$ mouse lines were separately prepared (Supplemental Fig. S5A,B). In the rescue experiment, the deletion allele was transmitted from sperm, because the oocytes were derived from the *Eed/Xist* DKO line (Fig. 5A). C-section at term followed by genotyping for the deletion alleles allowed us to compare the placental sizes between *Eed/Xist* matDKO with and without deletion alleles of each imprinted gene (Fig. 5A). Reverse transcription followed by quantitative PCR (RT-qPCR) analysis confirmed that the expression levels of all seven imprinted genes and C2MC-harboring miRNAs in *Eed/Xist* matDKO placentae are higher than those in WT placentae, and the up-regulation is largely suppressed by heterozygous deletion of the corresponding genes (Supplemental Fig. S6A,B). Furthermore, deletion of the *Sfmbt2*-CDS did not affect the expression of C2MC-harboring miRNAs and vice versa (Supplemental Fig. S6C,D). Consequently, we found that C2MC$^{+/\Delta}$ and *Slc38a4*$^{+/\Delta}$ significantly rescued the placental enlargement phenotype of the *Eed/Xist* matDKO concepti (Fig. 5B; Table 1). HE and PAS staining confirmed that invasion of the ST layer into the labyrinth layer is suppressed by C2MC$^{+/\Delta}$ or *Slc38a4*$^{+/\Delta}$ (Fig. 5C; Supplemental Fig. S6E). *Gm32885*$^{+/\Delta}$ also ameliorated the placental enlargement (Fig. 5B; Table 1). In contrast, *Gab1*$^{+/\Delta}$, *Jade1*$^{+/\Delta}$, *Platr20*$^{+/\Delta}$, *Sfmbt2*-CDS$^{+/\Delta}$, and *Smoc1*$^{+/\Delta}$ did not decrease the placental weights of *Eed/Xist* matDKO concepti (Fig. 5B; Table 1). These results suggest that LOI of C2MC, *Slc38a4*, and *Gm32885* contributes to placental enlargement in *Eed/Xist* matDKO embryos.

Discussion

Since the recent discovery of noncanonical imprinting, two LOI models have been generated: *Eed* matKO (Inoue et al. 2018; Prokopuk et al. 2018; Harris et al. 2019) and *Pcgf1/6* matKO (Mei et al. 2021). Both models showed transient *Xist* derepression at preimplantation, developmental retardation at postimplantation, biallelic expression of autosomal noncanonical imprinted genes in the extraembryonic cells, and prenatal sublethality. Furthermore, the *Pcgf1/6* matKO exhibited placental enlargement (Mei et al. 2021). However, the molecular relationship between LOI and these phenotypes has been overlooked. The present study provided genetic evidence that the developmental retardation and sublethality after implantation are mainly caused by *Xist* LOI and that the placental enlargement is caused by LOI of several autosomal genes.

Given that *Xist* LOI induces aberrant XCI only transiently at preimplantation in *Eed* matKO embryos, it remained unclear whether *Xist* imprinting is relevant to development. This is even more questionable when considering species-specific dynamics of XCI (Okamoto et al. 2011, 2021). For example, *Xist* is biallelically expressed and both X chromosomes are transiently silenced in rabbit preimplantation embryos (Okamoto et al. 2011), which recapitulate the phenotype of *Eed* matKO mouse embryos. Our data now demonstrate that prevention of ectopic *Xist* expression at the preimplantation stages greatly restores postimplantation development of *Eed* matKO embryos. This finding indicates that transient *Xist* imprinting before implantation is indeed developmentally important in mice. This notion is further supported by studies of somatic cell nuclear transfer (SCNT) embryos in which *Xist* is aberrantly expressed during preimplantation development: Knockdown (KD) of *Xist* in male SCNT embryos or the use of *Xist* KO male donor cells or *Xist* heterozygous KO female donor cells for SCNT prevents aberrant *Xist* expression and increases the developmental ratio (Inoue et al. 2010; Matoba et al. 2011, 2018). Nevertheless, because SCNT involves various epigenetic errors other than defective noncanonical imprinting, and the great majority (>80%) of SCNT embryos die even when using *Xist* KO donors (Gao et al. 2018; Matoba and Zhang 2018; Yang et al. 2021), the *Eed* matKO model provides clearer evidence for the requirement of *Xist* imprinting in natural development. Since some *Eed/Xist* matDKO embryos still suffer from postimplantation lethality, understanding the detailed mechanisms of the defects in *Eed/Xist* matDKO embryos might contribute to improvement of animal cloning technology in the future. Furthermore, how nonrodent species, such as rabbits, cope with transient biallelic XCI is a fascinating question.

Placental enlargement is also commonly observed in SCNT and *Eed* matKO embryos (Matoba and Zhang 2018). We previously showed that heterozygous KO of C2MC ameliorates placental enlargement in SCNT embryos (Inoue et al. 2020). KO of C2MC-harboring miRNA target gene candidates, such as follistatin (*Fst*), BMP-binding endothelial regulator (*Bmper*), and CCAAT enhancer binding protein β (*Cebpb*), in fertilized embryos results in enlargement of the ST layers in the placentae (Inoue et al. 2020). This suggests that dosage regulation of the C2MC-harboring miRNAs is important for controlling cell proliferation in the ST layer. A related study also showed that combinatorial heterozygous KO of *Sfmbt2*, *Gab1*, *Jade1*, and *Smoc1* suppresses placental enlargement in SCNT embryos, yet it is unknown whether expression of the C2MC-harboring miRNAs is impaired on the *Sfmbt2* KO allele (Wang et al. 2020). Importantly, unlike SCNT models, the present study enabled us to obtain a relatively large number of concepti (3.3–11.0) in a litter in which both WT and heterozygous KO concepti of a targeted imprinted gene are present. This was not possible in SCNT, where only one to two concepti were obtained in a

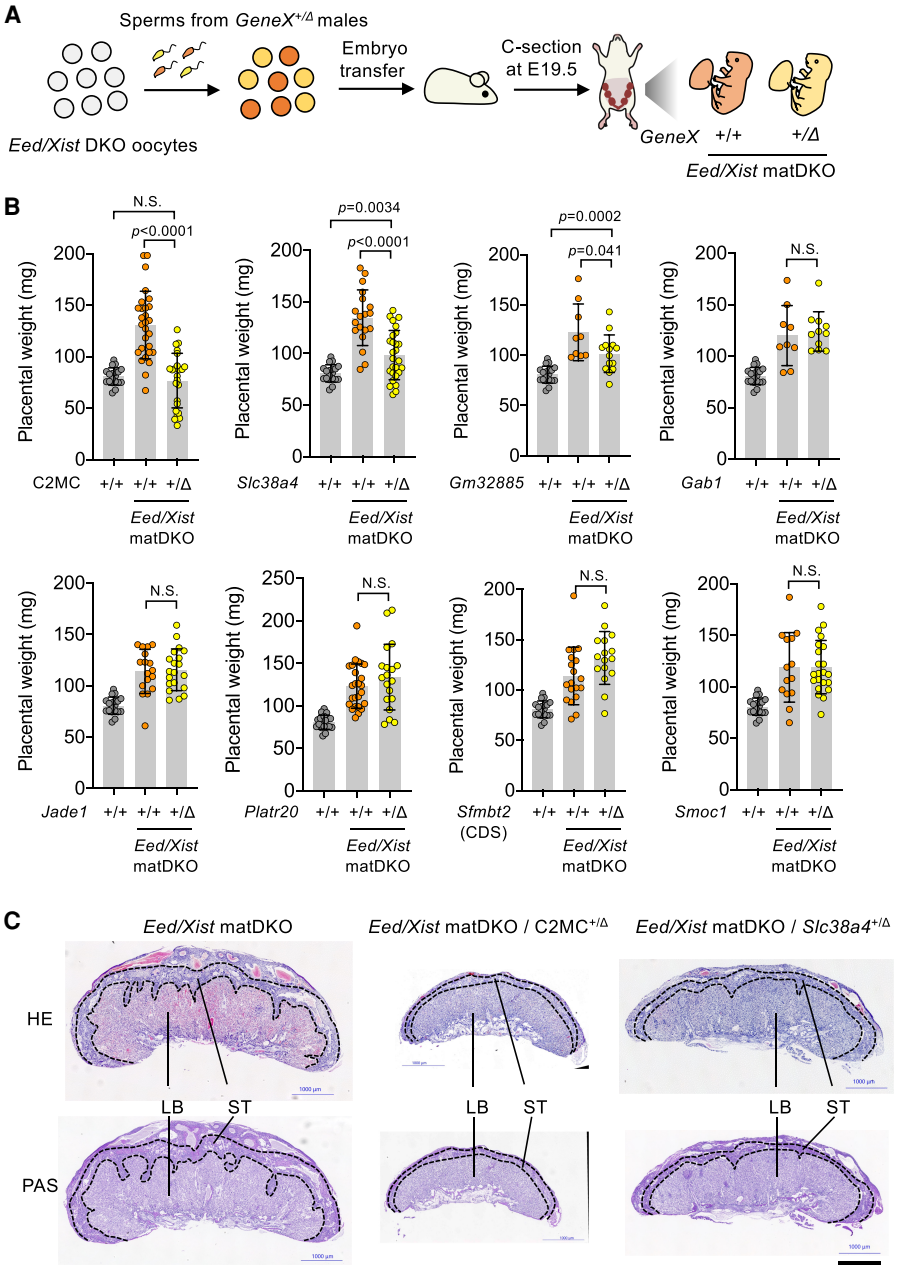

Figure 5. Heterozygous KO of autosomal noncanonical imprinted genes suppresses the placental enlargement in *Eed/Xist* matKO concepti. (*A*) Experimental scheme of the rescue experiment. *GeneX* represents one of the autosomal noncanonical imprinted genes. Genotyping of the *GeneX* KO allele distinguishes between +/+ and +/Δ fetuses. (*B*) Placental weights of *Eed/Xist* matDKO concepti with (+/Δ) or without (+/+) deletion alleles of the indicated genes. The *left* bars (+/+) indicate placental weights of WT concepti. The error bars overlaid on the plots indicate mean ± SD. The numbers of litters and concepti are indicated in Table 1. *P*, two-tailed Student's *t*-test. (*C*) Representative images of placental sections stained with hematoxylin and eosin (HE) and periodic acid Schiff (PAS). (LB) Labyrinthine layer, (ST) spongiotrophoblast layer. Scale bar, 1 mm. The numbers of placentae examined were four *Eed/Xist* matDKO, seven *Eed/Xist* matDKO/C2MC$^{+/\Delta}$, and four *Eed/Xist* matDKO/*Slc38a4*$^{+/\Delta}$.

litter (Inoue et al. 2020; Wang et al. 2020). Since litter sizes are known to affect the placental sizes, particularly when the number of concepti is small (McLaren 1965), rescue effects might be overlooked or misidentified by the confounding factor in SCNT of extremely small litter size. Therefore, the SCNT model alone was not sufficient, but complimenting approaches were needed to draw a solid conclusion. In this regard, the present study is valuable, as it validated the rescue effect by C2MC heterozygous KO in the *Eed/Xist* matDKO model.

In addition to C2MC, heterozygous KO of *Slc38a4* or *Gm32885* also partially suppresses placental

Table 1. *Summary of the placental rescue experiment*

Oocyte	Sperm	Number of litters	Total number of fetuses (Average ± SD)	Genotype of fetuses		Number of fetuses of the indicated genotype	Placental weight (mg) (Average ± SD)	Body weight (g) (Average ± SD)
WT	B6	3	20 (6.7 ± 2.1)	WT[a]		20/20 (100%)	80.7 ± 8.4	1.53 ± 0.12
Eed/Xist DKO	C2MC$^{+/\Delta}$	12	57 (4.8 ± 2.5)	*Eed/Xist* matDKO	C2MC$^{+/+}$	28/52 (54%)	130.6 ± 32.8	1.50 ± 0.12
					C2MC$^{+/\Delta}$	24/52 (46%)	76.7 ± 26.6[b]	1.28 ± 0.24[c]
	Slc38a4$^{+/\Delta}$	7	49 (7.0 ± 2.7)		*Slc38a4*$^{+/+}$	19/46 (41%)	134.6 ± 27.0	1.47 ± 0.14
					Slc38a4$^{+/\Delta}$	27/46 (59%)	98.5 ± 23.9[b]	1.36 ± 0.20[d]
	Gm32885$^{+/\Delta}$	4	23 (5.8 ± 1.3)		*Gm32885*$^{+/+}$	9/23 (39%)	122.7 ± 28.2	1.51 ± 0.16
					Gm32885$^{+/\Delta}$	14/23 (61%)	101.5 ± 18.7[d]	1.60 ± 0.12
	Gab1$^{+/\Delta}$	6	20 (3.3 ± 1.2)		*Gab1*$^{+/+}$	9/20 (45%)	120.0 ± 29.2	1.50 ± 0.17
					Gab1$^{+/\Delta}$	11/20 (55%)	124.0 ± 19.1	1.44 ± 0.16
	Jade1$^{+/\Delta}$	5	37 (7.4 ± 4.0)		*Jade1*$^{+/+}$	17/37 (46%)	114.1 ± 21.5	1.46 ± 0.16
					Jade1$^{+/\Delta}$	20/37 (54%)	115.7 ± 20.4	1.49 ± 0.12
	Platr20$^{+/\Delta}$	4	44 (11.0 ± 3.2)		*Platr20*$^{+/+}$	25/44 (57%)	123.3 ± 26.0	1.37 ± 0.12
					Platr20$^{+/\Delta}$	19/44 (43%)	133.8 ± 38.6	1.45 ± 0.16
	Sfmbt2-CDS$^{+/\Delta}$	6	37 (6.2 ± 1.2)		*Sfmbt2-CDS*$^{+/+}$	19/35 (54%)	113.9 ± 28.6	1.38 ± 0.17
					Sfmbt2-CDS$^{+/\Delta}$	16/35 (46%)	131.8 ± 26.2	1.31 ± 0.12
	Smoc1$^{+/\Delta}$	5	36 (7.2 ± 3.6)		*Smoc1*$^{+/+}$	14/36 (39%)	118.9 ± 33.8	1.34 ± 0.21
					Smoc1$^{+/\Delta}$	22/36 (61%)	119.1 ± 25.9	1.31 ± 0.14

[a]WT embryos were generated by IVF of *Eed*$^{fl/fl}$/*Xist*$^{fl/fl}$ oocytes and B6 sperm.
[b]$P < 0.0001$
[c]$P < 0.001$
[d]$P < 0.05$

enlargement. *Slc38a4* encodes a system A amino acid transporter, SNAT4. It is widely expressed in trophoblasts at the maternal–fetal interface in placentae, and its KO severely impairs placental development (Matoba et al. 2019). Since LOI of *Slc38a4* alone did not seem to affect the placental development (Bogutz et al. 2020), it might be required for placental enlargement. During the revision of this report, it was demonstrated that up-regulation of *Slc38a4* increases amino acid transport and overactivates the mechanistic target of rapamycin complex 1 (mTORC1) signaling pathway in SCNT placentae and that heterozygous KO of *Slc38a4* partially suppresses placental enlargement in SCNT (Xie et al. 2022). *Gm32885* is a predicted long noncoding RNA gene with unknown function. The molecular details of how imprints of these genes regulate placental development and whether placental enlargement affects their functions await further investigation.

The fact that loss of noncanonical imprinting causes placental enlargement is of great interest from an evolutionary point of view, as it supports the genetic conflict theory that was originally based on the functions of several canonical imprinted genes (Moore and Haig 1991). According to this theory, PEGs make the fetus and placenta grow bigger, while maternally expressed genes (MEGs) make them grow moderately to reduce maternal resource consumption during pregnancy. Although fetal growth was not enhanced in *Eed* and *Eed/Xist* matKO conditions, we speculate that placental enlargement might be beneficial for fetal growth under certain circumstances. In support of this idea, we observed that heterozygous KO of C2MC or *Slc38a4* led to reduction of the body weights accompanied by reduction of the placental weights (Table 1; Supplemental Fig. S7). This suggests that placental overgrowth had a positive effect on fetal growth in *Eed/Xist* matDKO concepti. Notably, noncanonical imprints at both autosomal genes and *Xist* appear to be acquired in rodents (Lehnert et al. 2011; Wang et al. 2011; Zheng et al. 2011; Bogutz et al. 2020; Lu et al. 2021). In this regard, it is intriguing to speculate that autosomal noncanonical imprinting might have evolved as a backup system to compensate fetal growth retardation even under an unwanted situation of *Xist* LOI. Future studies are warranted to understand why the noncanonical imprinting system evolved and how its placenta-specific feature is beneficial for development.

Materials and methods

Animal care

All animal experiments were performed in accordance with guidelines of the Institutional Animal Care and Use Committee at RIKEN Center for Integrative Medical Sciences and RIKEN

Bioresource Research Center. Same-sex littermates were housed in groups of up to five mice per ventilated cage with nesting materials. The mouse facility was kept at 21°C–25°C and 40%–60% humidity with a 12-h light and dark cycle.

Generation of oocyte-specific Eed/Xist *double conditional KO mutants*

The *Eed*^{flox} (B6;129S1-Eed^{tm1Sho}/J [022727]) and *Gdf9*^{Cre} [Tg (Gdf9-icre)5092Coo/J (011062)] mouse lines were originated from the Jackson Laboratory, and *Gdf9*^{Cre}/*Eed*$^{flox/flox}$ mice were previously generated (Inoue et al. 2018). The *Xist*^{flox} mouse line was initially generated by Csankovszki et al. (1999) and was maintained on a mixed background. After backcrossing to C57BL/6NCrl (B6N) males (Oriental Yeast) for two generations, *Xist*$^{+/flox}$ females were crossed with *Gdf9*^{Cre}/*Eed*$^{flox/flox}$ males to generate *Gdf9*^{Cre}/*Eed*$^{+/flox}$/*Xist*$^{flox/Y}$ males and *Eed*$^{+/flox}$/*Xist*$^{+/flox}$ females. They were intercrossed to obtain *Gdf9*^{Cre}/*Eed*$^{flox/flox}$/*Xist*$^{flox/Y}$, *Gdf9*^{Cre}/*Eed*$^{flox/flox}$/*Xist*$^{+/Y}$, and *Gdf9*^{Cre}/*Eed*$^{+/+}$/*Xist*$^{flox/Y}$ males and *Eed*$^{flox/flox}$/*Xist*$^{flox/flox}$, *Eed*$^{flox/flox}$/*Xist*$^{+/flox}$, and *Eed*$^{+/+}$/*Xist*$^{flox/flox}$ females. They were further intercrossed to obtain *Eed*$^{flox/flox}$/*Xist*$^{flox/flox}$ (WT), *Gdf9*^{Cre}/*Eed*$^{flox/flox}$/*Xist*$^{flox/flox}$ (DKO), *Gdf9*^{Cre}/*Eed*$^{flox/flox}$/*Xist*$^{+/+}$ (*Eed* KO), and *Gdf9*^{Cre}/*Eed*$^{+/+}$/*Xist*$^{flox/flox}$ (*Xist* KO) females for experiments. The tail tips were used for genotyping. The primer sets used for the *Xist* flox allele were Xist-2f-F2 and Xist-2f-R2, and those for the *Xist* deletion (Δ) allele were Xist-17(+) and Xist-1lox-F. The primer sequences are listed in Supplemental Table S2. By genotyping the *ΔXist* allele in embryos derived from *Gdf9*^{Cre}/*Eed*$^{flox/flox}$/*Xist*$^{flox/flox}$ and *Gdf9*^{Cre}/*Eed*$^{+/+}$/*Xist*$^{flox/flox}$ females, we confirmed that the frequency of *Gdf9*^{Cre}-mediated deletion of *Xist* was >98%.

Collection of mouse oocytes and preimplantation embryos

The procedures of GV and MII oocyte collection and in vitro fertilization (IVF) were described previously (Inoue et al. 2017a). GV oocytes were obtained from 8- to 12-wk-old females injected with pregnant mare serum gonadotropin (PMSG) 46–48 h before the collection. MII oocytes were obtained from PMSG- and human chorionic gonadotropin (hCG)-injected 8- to 12-wk-old females. Sperm used for IVF in the RNA-FISH experiment were harvested from B6D2F1 males (Oriental Yeast).

Whole-mount immunostaining

GV oocytes were fixed with 3.7% paraformaldehyde for 20 min at room temperature. After three washes with PBS containing 1% BSA (PBS/BSA), the oocytes were permeabilized by 0.5% Triton X-100 for 15 min at room temperature and then treated with mouse anti-H3K27me3 (1:500; MBL 323A) and rabbit anti-Eed antibodies (1:50; Cell Signaling Technology 85322) overnight at 4°C. After washing with PBS/BSA, they were incubated with a 1:250 dilution of Alexa Flour 488 donkey antimouse IgG and Alexa Flour 568 donkey antirabbit IgG (Life Technologies) for 1 h at room temperature. The samples were washed three times and then mounted on a glass slide in VectaShield antibleaching solution with 4′,6-diamidino-2-phenylindole (DAPI) (Vector Laboratories). Fluorescence was detected under a confocal microscope (Leica TCS Sp8). All images were acquired and quantified using LASX software (Leica). Briefly, the nuclear signal intensity of oocytes was determined, and the cytoplasmic signal was subtracted as background. Then, the average signal intensity of the WT oocytes was set as 1.0.

Whole-mount RNA/DNA fluorescent in situ hybridization

The procedures of probe preparation and the FISH experiment were described previously (Inoue et al. 2017b). Morula embryos were obtained by IVF and fixed at 72 hpf. As the marker of the X-chromosome location, a Green-dUTP probe made from a BAC clone containing the *Atrx* locus was used in the present study.

Caesarian section and placental histology

Females were cocaged with B6N males, and the presence of plugs was checked on a daily basis. The day of plug was counted as embryonic day (E) 0.5. Pregnant females were dissected at E6.5, E10.5, E13.5, and E18.5. After counting the numbers of implantation sites and fetuses and measuring the sizes or weights of fetuses and placentae, the placentae were fixed in 4% PFA overnight at 4°C. The samples were then routinely embedded in paraffin. Serial sections (5-µm thickness) were subjected to HE and PAS staining.

Rescue experiments by heterozygous KO of individual noncanonical imprinted genes

The *Gab1*$^{+/\Delta}$ mouse line was provided by RIKEN Bioresource Research Center through the National BioResource Project of the Ministry of Education, Culture, Sports, Science, and Technology/Agency for Medical Research and Development, Japan (RBRC00440) (Itoh et al. 2000). The C2MC$^{+/\Delta}$, *Slc38a4*$^{+/\Delta}$, and *Sfmbt2*-CDS$^{+/\Delta}$ mouse lines were generated previously (Inoue et al. 2017c, 2020; Matoba et al. 2019).

The *Gm32885*$^{+/\Delta}$, *Jade1*$^{+/\Delta}$, *Platr20*$^{+/\Delta}$, and *Smoc1*$^{+/\Delta}$ mouse lines were generated by CRISPR/Cas9 in this study (Supplemental Fig. S5). For *Gm32885* and *Platr20*, two sgRNAs per gene were designed to target flanking loci of the entire gene bodies. For *Jade1* and *Smoc1*, two sgRNAs per gene were designed to target flanking loci of exons 6–9 and exons 2–5, respectively: *Jade1* encodes a protein of 834 amino acids, and deletion of exons 6–9 results in the appearance of a stop codon at position amino acid 177. *Smoc1* encodes a protein of 463 amino acids, and deletion of exons 2–5 results in appearance of a stop codon at position amino acid 39. The sequences of the sgRNA targets were as follows: *Gm32885* (CTAAGTTGAATATTAACCCA and TGTCCTAC CAGGAGACGATT), *Jade1* (TTCCTTGTGTTTGCCGCTCG and GTGTGGCGCGCATCCCTCTC), *Platr20* (GTGCTAGCT TGGGCCACTAC and TACCTACTCCGTGAGCGGGC), and *Smoc1* (ATCTTTGGGATGCATACGGG and ATCATGGAA AAGGTCGGGGC). The sgRNAs were produced by using GeneArt Precision gRNA synthesis kit (Thermo Fisher). Cas9 nuclease (100 ng/µL; Integrated DNA Technologies) and sgRNAs (50 ng/µL each) were injected into the cytoplasm of B6N × B6N or BDF1 × B6N zygotes. The embryos were transferred into surrogate ICR females, and founder mice were obtained. After PCR validation and Sanger sequencing to determine the precise deletion sizes of the KO alleles, the founders were backcrossed to B6N for at least two generations. The genotyping primers for detecting these KO alleles were Gm32885-KO-F/R, Jade1-KO-F/R, Platr20-KO-F/R, and Smoc1-KO-F/R (Supplemental Table S2). Primer sequences for the other KO lines are also listed in Supplemental Table S2.

For the rescue experiment, the *Eed*/*Xist* double flox line was further backcrossed to B6N males for a total of six generations. Then, *Eed*$^{+/flox}$/*Xist*$^{+/flox}$ females were crossed with a *Zp3*^{Cre} mouse line (C57BL/6-Tg(Zp3-cre)93Knw/J; The Jackson Laboratory 003651). The offspring were intercrossed to obtain *Zp3*^{Cre}/*Eed*$^{flox/flox}$/*Xist*$^{flox/flox}$ (DKO) and *Eed*$^{flox/flox}$/*Xist*$^{flox/flox}$ (WT) females. The primers detecting the *Zp3*^{Cre} were described

previously (Mei et al. 2021). For IVF, 8- to 12 wk-old females were injected with 7.5 IU of PMSG or 0.15 mL of CARD HyperOva (Kyudo Co., Ltd.) followed by 7.5 IU of hCG 48 h later. MII oocytes were obtained from these females and inseminated with sperm obtained from the heterozygous KO males. After culturing fertilized oocytes in KSOM in a humidified atmosphere with 5% CO_2/95% air at 37°C, two-cell embryos were transferred into surrogate ICR strain mothers. C-section was performed at E19.5.

RNA-seq for morula embryos

To prepare *Eed*/*Xist* matDKO and control embryos, the above-described $Zp3^{Cre}/Eed^{flox/flox}/Xist^{flox/flox}$ (DKO) and $Eed^{flox/flox}/Xist^{flox/flox}$ (WT) females were used. To prepare *Eed* matKO and control embryos, we generated $Zp3^{Cre}/Eed^{flox/flox}$ (KO) and $Eed^{flox/flox}$ (WT) females by backcrossing the $Gdf9^{Cre}/Eed^{flox/flox}$ mice (Inoue et al. 2018) to B6N for two generations followed by crossing with the $Zp3^{Cre}$ line. To generate F1 hybrid embryos, 8- to 12-wk-old females were injected with 0.2 mL of CARD HyperOva followed by 7.5 IU of hCG at a 48-h interval. Cumulus–oocyte complexes (COCs) were harvested 15–17 h after hCG injection and inseminated with activated spermatozoa in HTF medium supplemented with 10 mg/mL bovine serum albumin (BSA; Merck Millipore 12657). Sperms were obtained from the caudal epididymis of adult PWK/PhJ mice (RBRC00213 [RIKEN Bioresource Research Center] originated from 003715 [the Jackson Laboratory]). Spermatozoa were capacitated by 1-h incubation in CARD FertiUp (Kyudo Co., Ltd.). At 6 h postinsemination (hpi), zygotes with two pronuclei were transferred to KSOM and cultured in a humidified atmosphere with 5% CO_2/95% air at 37.8°C. At 79 hpi, morula embryos were treated with acidic Tyrode's solution to remove zona pellucida, washed in M2 media (Merck Millipore MR-015-D), and then washed in 0.2% BSA/PBS. Five embryos per sample were pooled in *Eed* matKO and WT embryos, and 13 embryos per sample were pooled in *Eed*/*Xist* matDKO and WT embryos. RNA-seq libraries were prepared with biological duplicates and sequenced as described previously (Mei et al. 2021).

RNA-seq data analysis

All RNA-seq reads were trimmed using Fastp (version 0.21.0) (Chen et al. 2018). For allelic analysis, B6/129 and PWK SNPs were masked as "N" in the mouse reference genome (mm10). Reads after trimming were mapped to the "N"-masked reference genome using STAR (version 2.7.6a) (Dobin et al. 2013) with parameters "–runMode alignReads –alignEndsType EndToEnd –outSAMattributes NH NI NM MD –outSAMtype BAM Unsorted." After the removal of PCR duplicates using picard-tools (version 1.119; http://broadinstitute.github.io/picard) with the parameters "-Xms12G -Xmx14G -jar MarkDuplicates.ja," these uniquely aligned reads were used to determine the parental origins using SNPsplit (version 0.4.0; https://f1000research.com/articles/5-1479/v2). To analyze gene expression changes in RNA-seq, raw read counts for each gene were calculated using featureCounts (version 2.0.1) (Liao et al. 2014) with the parameters "-p -s 0 -t exon -g gene_id." Genes with ≥20 single-nucleotide polymorphism (SNP) reads in all replicates were subjected to downstream analyses.

To define PEGs, we first used previously published RNA-seq data sets of B6 × PWK and PWK × B6 morula embryos (Mei et al. 2021). Genes with ≥20 SNP-containing reads in Rep1+2 in both reciprocal crosses were analyzed, and those showing paternal expression biases [FC(Pat/Mat) ≥ 1.5] in both reciprocal crosses were considered as candidate PEGs. Then, genes showing FC(Pat/Mat) ≥ 2.0 in all replicates of *Eed* WT and *Eed*/*Xist* WT samples were identified as PEGs. Among these PEGs, those losing paternal expression biases in *Eed* matKO embryos were defined as H3K27me3-dependent genes [averaged FC(Pat/Mat) < 1], and those losing paternal expression biases in *Dnmt3l* matKO embryos were defined as DNA methylation-dependent genes (Chen et al. 2019). All of the RNA-seq data sets generated in this study were deposited to the Gene Expression Omnibus database under accession number GSE199115.

Quantitative reverse transcription PCR

Total RNA was extracted from placentae by using TRIzol reagent (Thermo Fisher Scientific). For mRNA quantification, cDNAs were synthesized by SuperScript IV first-strand synthesis system (Thermo Fisher Scientific 18091050). Quantitative PCR was performed by using PowerUp SYBR Green master mix (Thermo Fisher Scientific) in QuantStudio 7 Flex system (Thermo Fisher Scientific). The Ct values were normalized to that of β actin. The primer sequences are in Supplemental Table S2.

For miRNA quantification, miRNAs were isolated from the extracted total RNA by using mirVana miRNA isolation kit (Thermo Fisher). Reverse transcription was performed by using a TaqMan microRNA reverse transcription kit (Thermo Fisher). QuantiTect probe PCR kits (Qiagen) with primers from TaqMan microRNA assays (Thermo Fisher) were used for quantification of miRNA. The Ct values were normalized to that of the U6 snRNA. Assay IDs were as follows: 001671 for *miR467a-5p*, 464179_mat for *miR467a-3p*, 464896_mat for *miR466b-3p*, and 001973 for U6 snRNA. Each experiment was performed in technical duplicates with three placentae per group.

Competing interest statement

The authors declare no competing interests.

Acknowledgments

We thank members of the animal facility of RIKEN Center for Integrative Medical Sciences who helped with the embryo transfer experiments, the Haruhiko Koseki laboratory members for helpful discussion, and Tadashi Yamamoto and Kazuhiko Yamamoto (RIKEN) for support of our Young Chief Investigator program project. This project was partly supported by the Ministry of Education, Culture, Sports, Science, and Technology (MEXT) Leading Initiative for Excellent Young Researchers grant to A.I., Japan Society for the Promotion of Science (JSPS) Grants-in-Aid for Scientific Research KAKENHI (18H02359 to A.I. and 20H03159 to S.M.), Grants-in-Aid for Scientific Research on Innovative Areas (19H05754 to A.I. and 19H05758 to A.O.), Grant-in-Aid for Early-Career Scientist (19K17971 to C.K.), and Grant-in-Aid for JSPS Fellows (20J21541 to R.H.); the Japan Foundation for Applied Enzymology to C.K.; the Japan Agency for Medical Research and Development PRIME (JP18gm6110012 and JP20gm6110012 to A.I.); the Uehara Memorial Foundation to A.I.; and intramural grants within RIKEN, including the All-RIKEN "Epigenome Manipulation Project" and the RIKEN Pioneering Project "Genome Building from TADs" to A.I. and A.O.

Author Contributions: A.I. conceived the project. S.M. and A.I. designed the experiments. S.M., C.K., M.K., K.I., and A.I. performed the experiments. R.H. analyzed sequencing data. S.M., C.K., and A.I. interpreted the data. S.M., K.M., K.I., and A.O. provided the heterozygous KO mouse lines of noncanonical

imprinted genes. T.O. provided the *Xist* flox mice. S.M. and A.I. wrote the manuscript.

References

Andergassen D, Smith ZD, Kretzmer H, Rinn JL, Meissner A. 2021. Diverse epigenetic mechanisms maintain parental imprints within the embryonic and extraembryonic lineages. *Dev Cell* **56:** 2995–3005.e4. doi:10.1016/j.devcel.2021.10.010

Augui S, Nora EP, Heard E. 2011. Regulation of X-chromosome inactivation by the X-inactivation centre. *Nat Genet* **12:** 429–442. doi:10.1038/nrg2987

Bogutz AB, Brind'Amour J, Kobayashi H, Jensen KN, Nakabayashi K, Imai H, Lorincz MC, Lefebvre L. 2020. Evolution of imprinting via lineage-specific insertion of retroviral promoters. *Nat Commun* 1–28.

Chen Z, Zhang Y. 2020. Maternal H3K27me3-dependent autosomal and X chromosome imprinting. *Nat Rev Genet* **21:** 555–571. doi:10.1038/s41576-020-0245-9

Chen S, Zhou Y, Chen Y, Gu J. 2018. Fastp: an ultra-fast all-in-one FASTQ preprocessor. *Bioinformatics* **34:** i884–i890. doi:10.1093/bioinformatics/bty560

Chen Z, Yin Q, Inoue A, Zhang C, Zhang Y. 2019. Allelic H3K27me3 to allelic DNA methylation switch maintains noncanonical imprinting in extraembryonic cells. *Sci Adv* **5:** eaay7246. doi:10.1126/sciadv.aay7246

Csankovszki G, Panning B, Bates B, Pehrson JR, Jaenisch R. 1999. Conditional deletion of Xist disrupts histone macroH2A localization but not maintenance of X inactivation. *Nat Genet* **22:** 323–324. doi:10.1038/11887

Dobin A, Davis CA, Schlesinger F, Drenkow J, Zaleski C, Jha S, Batut P, Chaisson M, Gingeras TR. 2013. STAR: ultrafast universal RNA-seq aligner. *Bioinformatics* **29:** 15–21. doi:10.1093/bioinformatics/bts635

Du Z, Zheng H, Kawamura YK, Zhang K, Gassler J, Powell S, Xu Q, Lin Z, Xu K, Zhou Q, et al. 2020. Polycomb group proteins regulate chromatin architecture in mouse oocytes and early embryos. *Mol Cell* **77:** 825–839.e7. doi:10.1016/j.molcel.2019.11.011

Gao R, Wang C, Gao Y, Xiu W, Chen J, Kou X, Zhao Y, Liao Y, Bai D, Qiao Z, et al. 2018. Inhibition of aberrant DNA re-methylation improves post-implantation development of somatic cell nuclear transfer embryos. *Cell Stem Cell* **23:** 426–435.e5. doi:10.1016/j.stem.2018.07.017

Hanna CW, Kelsey G. 2021. Features and mechanisms of canonical and noncanonical genomic imprinting. *Genes Dev* **35:** 821–834. doi:10.1101/gad.348422.121

Hanna CW, Pérez-Palacios R, Gahurova L, Schubert M, Krueger F, Biggins L, Andrews S, Colomé-Tatché M, Bourc'his D, Dean W, et al. 2019. Endogenous retroviral insertions drive non-canonical imprinting in extra-embryonic tissues. *Genome Biol* **20:** 225. doi:10.1186/s13059-019-1833-x

Harris C, Cloutier M, Trotter M, Hinten M, Gayen S, Du Z, Xie W, Kalantry S. 2019. Conversion of random X-inactivation to imprinted X-inactivation by maternal PRC2. *Elife* **8:** 166. doi:10.7554/eLife.44258

Inoue K, Kohda T, Sugimoto M, Sado T, Ogonuki N, Matoba S, Shiura H, Ikeda R, Mochida K, Fujii T, et al. 2010. Impeding *Xist* expression from the active X chromosome improves mouse somatic cell nuclear transfer. *Science* **330:** 496–499. doi:10.1126/science.1194174

Inoue A, Jiang L, Lu F, Suzuki T, Zhang Y. 2017a. Maternal H3K27me3 controls DNA methylation-independent imprinting. *Nature* **547:** 419–424. doi:10.1038/nature23262

Inoue A, Jiang L, Lu F, Zhang Y. 2017b. Genomic imprinting of *Xist* by maternal H3K27me3. *Genes Dev* **31:** 1927–1932. doi:10.1101/gad.304113.117

Inoue K, Hirose M, Inoue H, Hatanaka Y, Honda A, Hasegawa A, Mochida K, Ogura A. 2017c. The rodent-specific microRNA cluster within the Sfmbt2 gene is imprinted and essential for placental development. *Cell Rep* **19:** 949–956.

Inoue A, Chen Z, Yin Q, Zhang Y. 2018. Maternal *Eed* knockout causes loss of H3K27me3 imprinting and random X inactivation in the extraembryonic cells. *Genes Dev* **32:** 1525–1536. doi:10.1101/gad.318675.118

Inoue K, Ogonuki N, Kamimura S, Inoue H, Matoba S, Hirose M, Honda A, Miura K, Hada M, Hasegawa A, et al. 2020. Loss of H3K27me3 imprinting in the Sfmbt2 miRNA cluster causes enlargement of cloned mouse placentas. *Nat Commun* **11:** 2150. doi:10.1038/s41467-020-16044-8

Itoh M, Yoshida Y, Nishida K, Narimatsu M, Hibi M, Hirano T. 2000. Role of Gab1 in heart, placenta, and skin development and growth factor- and cytokine-induced extracellular signal-regulated kinase mitogen-activated protein kinase activation. *Mol Cell Biol* **20:** 3695–3704. doi:10.1128/MCB.20.10.3695-3704.2000

Kobayashi H. 2021. Canonical and Non-canonical genomic imprinting in rodents. *Front Cell Dev Biol* **9:** 713878. doi:10.3389/fcell.2021.713878

Lan ZJ, Xu X, Cooney AJ. 2004. Differential oocyte-specific expression of Cre recombinase activity in GDF-9-iCre, Zp3cre, and Msx2Cre transgenic mice. *Biol Reprod* **71:** 1469–1474. doi:10.1095/biolreprod.104.031757

Lee JT, Bartolomei MS. 2013. X-inactivation, imprinting, and long noncoding RNAs in health and disease. *Cell* **152:** 1308–1323. doi:10.1016/j.cell.2013.02.016

Lehnert S, Kapitonov V, Thilakarathne PJ, Schuit FC. 2011. Modeling the asymmetric evolution of a mouse and rat-specific microRNA gene cluster intron 10 of the Sfmbt2 gene. *BMC Genomics* **12:** 257. doi:10.1186/1471-2164-12-257

Liao Y, Smyth GK, Shi W. 2014. Featurecounts: an efficient general purpose program for assigning sequence reads to genomic features. *Bioinformatics* **30:** 923–930. doi:10.1093/bioinformatics/btt656

Loda A, Collombet S, Heard E. 2022. Gene regulation in time and space during X-chromosome inactivation. *Nat Rev Mol Cell Biol* **23:** 231-249. doi:10.1038/s41580-021-00438-7

Lu X, Zhang Y, Wang L, Wang L, Wang H, Xu Q, Xiang Y, Chen C, Kong F, Xia W, et al. 2021. Evolutionary epigenomic analyses in mammalian early embryos reveal species-specific innovations and conserved principles of imprinting. *Sci Adv* **7:** eabi6178. doi:10.1126/sciadv.abi6178

Matoba S, Zhang Y. 2018. Somatic cell nuclear transfer reprogramming: mechanisms and applications. *Cell Stem Cell* **23:** 471–485. doi:10.1016/j.stem.2018.06.018

Matoba S, Inoue K, Kohda T, Sugimoto M, Mizutani E, Ogonuki N, Nakamura T, Abe K, Nakano T, Ishino F, et al. 2011. RNAi-mediated knockdown of *Xist* can rescue the impaired postimplantation development of cloned mouse embryos. *Proc Natl Acad Sci* **108:** 20621–20626. doi:10.1073/pnas.1112664108

Matoba S, Wang H, Jiang L, Lu F, Iwabuchi KA, Wu X, Inoue K, Yang L, Press W, Lee JT, et al. 2018. Loss of H3K27me3 imprinting in somatic cell nuclear transfer embryos disrupts post-implantation development. *Cell Stem Cell* **23:** 343–354.e5. doi:10.1016/j.stem.2018.06.008

Matoba S, Nakamuta S, Miura K, Hirose M, Shiura H, Kohda T, Nakamuta N, Ogura A. 2019. Paternal knockout of *Slc38a4*/SNAT4 causes placental hypoplasia associated with

intrauterine growth restriction in mice. *Proc Natl Acad Sci* **116:** 21047–21053. doi:10.1073/pnas.1907884116

McLaren A. 1965. Genetic and environmental effects on foetal and placental growth in mice. *J Reprod Fertil* **9:** 79–98. doi:10.1530/jrf.0.0090079

Mei H, Kozuka C, Hayashi R, Kumon M, Koseki H, Inoue A. 2021. H2AK119ub1 guides maternal inheritance and zygotic deposition of H3K27me3 in mouse embryos. *Nat Genet* **53:** 539–550. doi:10.1038/s41588-021-00820-3

Moore T, Haig D. 1991. Genomic imprinting in mammalian development: a parental tug-of-war. *Trends Genet* **7:** 45–49. doi:10.1016/0168-9525(91)90040-W

Okamoto I, Patrat C, Thépot D, Peynot N, Fauque P, Daniel N, Diabangouaya P, Wolf JP, Renard JP, Duranthon V, et al. 2011. Eutherian mammals use diverse strategies to initiate X-chromosome inactivation during development. *Nature* **472:** 370–374. doi:10.1038/nature09872

Okamoto I, Nakamura T, Sasaki K, Yabuta Y, Iwatani C, Tsuchiya H, Nakamura SI, Ema M, Yamamoto T, Saitou M. 2021. The X chromosome dosage compensation program during the development of cynomolgus monkeys. *Science* **374:** eabd8887. doi:10.1126/science.abd8887

Prokopuk L, Stringer JM, White CR, Vossen RHAM, White SJ, Cohen ASA, Gibson WT, Western PS. 2018. Loss of maternal EED results in postnatal overgrowth. *Clin Epigenetics* **10:** 95. doi:10.1186/s13148-018-0526-8

Raas MWD, Zijlmans DW, Vermeulen M, Marks H. 2022. There is another: H3K27me3-mediated genomic imprinting. *Trends Genet* **38:** 82–96. doi:10.1016/j.tig.2021.06.017

Santini L, Halbritter F, Titz-Teixeira F, Suzuki T, Asami M, Ma X, Ramesmayer J, Lackner A, Warr N, Pauler F, et al. 2021. Genomic imprinting in mouse blastocysts is predominantly associated with H3K27me3. *Nat Commun* **12:** 3804. doi:10.1038/s41467-021-23510-4

Tucci V, Isles AR, Kelsey G, Ferguson-Smith AC, Erice Imprinting Group. 2019. Genomic imprinting and physiological processes in mammals. *Cell* **176:** 952–965. doi:10.1016/j.cell.2019.01.043

Wang Q, Chow J, Hong J, Smith AF, Moreno C, Seaby P, Vrana P, Miri K, Tak J, Chung ED, et al. 2011. Recent acquisition of imprinting at the rodent Sfmbt2 locus correlates with insertion of a large block of miRNAs. *BMC Genomics* **12:** 204. doi:10.1186/1471-2164-12-204

Wang LY, Li ZK, Wang LB, Liu C, Sun XH, Feng GH, Wang JQ, Li YF, Qiao LY, Nie H, et al. 2020. Overcoming intrinsic H3K27me3 imprinting barriers improves post-implantation development after somatic cell nuclear transfer. *Cell Stem Cell* **27:** 315–325.e5. doi:10.1016/j.stem.2020.05.014

Xie Z, Zhang W, Zhang Y. 2022. Loss of Slc38a4 imprinting is a major cause of mouse placenta hyperplasia in somatic cell nuclear transferred embryos at late gestation. *Cell Rep* **38:** 110407. doi:10.1016/j.celrep.2022.110407

Yang G, Zhang L, Liu W, Qiao Z, Shen S, Zhu Q, Gao R, Wang M, Wang M, Li C, et al. 2021. Dux-Mediated corrections of aberrant H3K9ac during 2-cell genome activation optimize efficiency of somatic cell nuclear transfer. *Cell Stem Cell* **28:** 150–163.e5. doi:10.1016/j.stem.2020.09.006

Zeng TB, Pierce N, Liao J, Szabo PE. 2021. H3k9 methyltransferase EHMT2/G9a controls ERVK-driven noncanonical imprinted genes. *Epigenomics* **13:** 1299–1314.

Zheng GX, Ravi A, Gould GM, Burge CB, Sharp PA. 2011. Genome-wide impact of a recently expanded microRNA cluster in mouse. *Proc Natl Acad Sci* **108:** 15804–15809. doi:10.1073/pnas.1112772108

Noncanonical imprinting sustains embryonic development and restrains placental overgrowth

Shogo Matoba, Chisayo Kozuka, Kento Miura, et al.

Genes Dev. published online April 28, 2022
Access the most recent version at doi:10.1101/gad.349390.122